PD.TVZ.HR
POLYTECHNIC & DESIGN Vol. 9, No. 3, 2021.
Mrežna inačica: ISSN 2459-6302
Tiskana inačica: ISSN 1849-1995
DOI: 10.19279/TVZ.PD.2021-9-3-11

DESIGN AND FABRICATION OF OPTIMISED AEROSTATIC DRY GAS SEALS USING ADVANCED NUMERICAL MODELS AND NEXT GENERATION PRODUCTION TECHNOLOGY

Schaham Schoar[1], Arno Elspaß[2], Hans Josef Dohmen[1], Stefan Kleszczynski[2], Friedrich-Karl Benra[1]

[1]University of Duisburg-Essen, Chair of Turbomachinery, Duisburg, Germany
[2]University of Duisburg-Essen, Chair of Manufacturing Technology, Duisburg, Germany

ABSTRACT

To avoid pollution of the environment, it is necessary to separate the oil of the oil- lubricated bearings of a turbomachine from the atmosphere. For this purpose, gas driven sealing systems which operate with a non- toxic gas are used. These sealing systems must be robust and reliable but also should have a low consumption of the operating gas to meet economic criteria. Furthermore, the seals should be tight without any operating medium when the turbomachine is at a standstill "blocked situation". All these requirements are combined in the so- called aerostatic seals which are used in the industry already. The robust aerostatic seals are manufactured conventionally by drilling a defined number of holes with fixed diameter in the seal sliding ring to ensure the permeability. The characteristic of the seals can be influenced in a certain spectrum by varying the number and the diameter of the holes. This effect has already been demonstrated by Gerke (1991), Schulz (1999) or Dormann (2002), among others. Actually, the possibilities of conventional manufacturing processes restrict the use of the complete potential of such seal types. An approach to increase the performance of this seals is the application of Additive Manufacturing (AM) processes directly during the design. It is widely accepted, that AM processes offer a great potential in terms of geometrical freedom and thus for optimised functionality. One of the main advantages of these AM processes is that exposure strategies which contain the typic process parameters can be set for each part separately. Furthermore, the technic offers a great potential for production of filigree structures. With these structures it is possible to manufacture a seal with the necessary permeability as well as dense material which serves as a mounting device.

As shown in a previous publication from Schoar et al. (2019), a numerical model which is required to support the design process of seals with undefined as well as defined distributed permeabilities has been derived and validated using a test bench. In this work, the AM process of laser-based powder bed fusion of metals is used to generate coaxial gas seals with defined permeability distributions according to the calculations of the numerical model. It is shown that the fabrication of AM dry gas seals with the required permeability distributions is possible. A comprehension of the results from the numerical model and the experiment proves, that the validated numerical model can be used for the design of seals with different permeabilities and thus for the aerostatic dry gas seals (ADGS).

Ključne riječi: *ADDITIVE MANUFACTURING, PBF- LB/M, STATIC SEAL, DRY GAS SEAL*

NOMENCLATURE

h	Gap height	[µm]
η	Dynamic viscosity	[Pa s]
k	Permeability	[m^2]
p	Pressure	[bar]
Q	Volume flow, related to Q_{max}	[-]
r	Radial direction	
R	Specific gas constant	[J/(kg K)]
R_n	Dimensionless radius	[-]
T	Temperature	[K]
w	Axial velocity	[m/s]
z	Axial direction	
v	Radial velocity	[m/s]

ABBREVIATIONS

ADGS	Aerostatic Dry Gas Seal
AM	Additive Manufacturing
DGS	Dry Gas Seal
FS	Full Scale
PBF-LB/M	Laser-Based Powder Bed Fusion of Metals

1. INTRODUCTION

In turbomachinery, seals are used to seal the gaps between rotating and stationary components. Leakage between rotating and stationary parts in turbomachinery has a strong impact on their performance and reliability. The demand for robust and reliable sealing solutions is therefore high. Aerostatic and aerodynamic acting gas seals are used to reduce leakages and friction losses, decreasing the efficiency of the entire system. These types of seals, as depicted in figure 1, form a sealing gap axially to the rotor axis which prevents mechanical contact between the rotating ring and the not rotating machine parts during operation. The height of the sealing gap changes during operation due to the process conditions. These seals are therefore assigned to the axial seal types and are referred to as active seals.

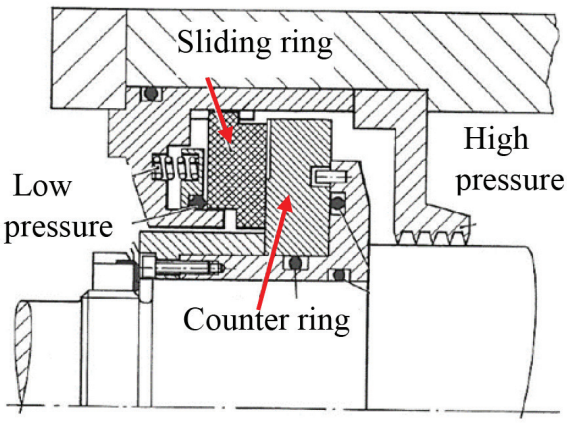

Figure 1 *Schematic representation of a DGS according to Launert (1994)*

In general, an aerostatic acting seal is pressurized with an operating gas through several bores distributed across the stationary ring. This gas causes a force between the stationary ring and the counter ring. Thus, a gap of approx. 10 µm between these rings is created.

The stationary ring of an aerostatic seal is movable in axial direction within a defined range and thus adjusts itself autonomously with regard to its force balance. Therefore, this is also referred to as the sliding ring. These characteristic properties have a positive effect on the overall operating behaviour of the seal. In the past it has been shown for example by Gerke (1991) that the use of permeable parts with distributed permeabilities improves the pressure profile in the gap with regard to its damping and stiffness properties, compared to parts with a few bores.

In this work, aerostatic acting gas seals with permeable distributions, which have not been a topic in research before, are investigated numerically. Furthermore, a test bench is designed and built for ADGS to validate the numerical model. In addition, permeable sliding rings which have three regions with material of different permeabilities are produced using the PBF- LB/M process. The permeability of the material in each region can be influenced during the design by varying the build-up strategy. In the process, the permeabilities are first determined numerically and the corresponding machine parameters are calculated. Subsequently, the sliding rings are designed and manufactured according to the numerical results. A major advantage is that the coefficient of permeability changes the point of attack of the resulting pressure force. In this way the deformation of the sliding ring and the counter ring at higher pressure levels can be mitigated.

2. STATE OF THE ART

While the use of permeable materials in gas seals is not covered in the relevant literature, studies on permeable materials in air bearings exist at least since the 1950s. Montgomery and Sterry (1955) consider permeable materials with regard to their applicability in air bearings in their work. Based on the Reynolds lubrication theory, Sneck (1963) succeeds in calculating the flow processes within permeable bearings. Schmidt (1972) describes the manufacturing and machining processes for porous air bearings, which are not investigated at that time. In his work, he shows the possibility of machining permeable materials without closing the pores at the machined surface.

In the following years, Majumnder and Majumdar (1988) develop a three-dimensional description of the flow processes in permeable air bearings. To simplify the calculation and design, Gerke (1991) provides a calibration method for various air bearing types, in order to calculate the axial and radial load capacity and stiffness as well as the tilting rigidity and the tilting moment as a function of bearing geometry, gap height, supply pressure and air consumption. His comparison of different types of bearings shows that sintered air bearings with micro jets distributed over the surface have the greatest load-bearing capacity and stiffness under the same boundary conditions. In the work of Schulz (1999) the machining of air bearings by laser is described. Furthermore, the comparison of different bearing types shows that the uniform nozzle distribution has the highest damping of vibrations occurring in the bearings. Dormann (2002) proves the work of Schulz and Gerke by investigating bearings with discrete nozzle distributions and compares them with sintered bearings.

For most of the calculations of a gas film in a gap between two components, Reynolds' lubrication theory is used as a basis until today. Reynolds' lubrication theory simplifies the continuity equation so that the pressure distribution in the gas film can be calculated as a function of a few characteristic parameters such as the gap height, the dynamic viscosity of the gas and the thermodynamic properties temperature and gas constant.

A first basis for the formulation of empirical momentum balances is provided by the experimental investigations of Henry Darcy (1856). According to his observations of the flow of water through a homogeneous sand bed, a linear relationship between the pressure gradient and the flow velocity relative to the cross-section of the soil sample is asserted. With the help of this finding, Darcy derives a resistance law at the end of the 19th century that reflects this relationship with a coefficient of permeability. The application of Darcy's law (Darcy equation) is limited to laminar and viscous flows.

3. THEORETICAL MODEL

In order to determine the characteristic values of the seal, such as leakage or gap height, the pressure distribution in the sliding ring and in the gap is calculated by means of simulation carried out for the case of not rotating machine parts (static simulation). For this purpose, the permeable sliding ring and the gap are defined as the calculation area. Based on the rotational symmetry of the sliding ring and the counter ring as well as the circumferentially symmetrical flow through the gap, a two- dimensional consideration is taken as a basis.

As derived in Schoar et al. (2019), the flow within the permeable sliding ring is assumed to be laminar and thus the Darcy equation is applied for the calculation as follows:

Axial velocity:

$$\mathrm{w(z)} = -\frac{k_z}{\eta}\frac{dp}{dz} \tag{1}$$

Radial velocity:

$$\mathrm{v}\,(r) = -\frac{k_r}{\eta}\frac{dp}{dr} \tag{2}$$

For this purpose, the Reynolds differential equation, which represents a partial linear differential equation of second order and corresponding to a parabolic type, is used in a cylindrical coordinate system. Thus, the equation for the flow through the permeable sliding ring can be derived:

$$r\frac{\partial}{\partial r}\left(-\frac{p}{R\cdot T}\cdot\frac{k_\mathrm{r}}{\eta}\cdot\frac{\partial p}{\partial r}\right) + \frac{\partial}{\partial z}\left(-\frac{p}{R\cdot T}\cdot\frac{k_\mathrm{z}}{\eta}\cdot\frac{\partial p}{\partial z}\right) = 0\ . \tag{3}$$

Here k_r describes the permeability coefficient in the radial direction (r- coordinate) in the sliding ring and k_z the value in the axial direction (z-coordinate), see figure 2.

To calculate the pressure distribution in the gap, the Reynolds differential equation is used and extended by an additional term. This part is depicted in red colour in the following equation:

$$r\frac{\partial}{\partial r}\left(\frac{p}{\mathrm{R}\cdot\mathrm{T}}\cdot\frac{h^3}{12\cdot\eta}\cdot\frac{\partial p}{\partial r}\right) + \frac{\partial}{\partial z}\left(-\frac{p}{R\cdot T}\cdot\frac{k_z}{\eta}\cdot\frac{\partial p}{\partial z}\right) = 0 \quad (4)$$

The first part of this equation represents the mass flow at the outlet in radial direction, and the second part (coloured red) represents the mass flow at the inlet of the gap coming through the permeable sliding ring.

4. TEST BENCH

Figure 2 shows the test bench in a sectional view with the components of the housing, the counter ring, the sliding ring and the indicated process flow (dark blue arrows).

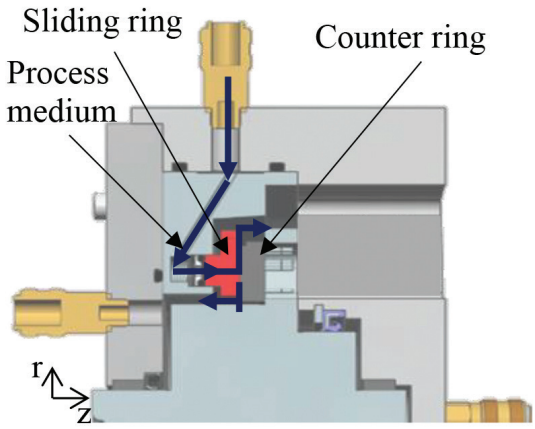

Figure 2 *Sectional view of the test bench*

The shaft, along with the counter ring (rotating ring in the machine), are mounted by means of plain bearings. The primary (porous) sliding ring / stationary ring, in a seal holder, is connected as a unit to the front of the shaft and fixed by means of the cover with bolts.

To measure the static pressure within the gap, three counter rings are manufactured conventionally (turning process, drilling, grinding, and polishing) with pressure holes as shown in figure 3.

The holes of 0.5 mm diameter are drilled into the counter ring to measure the static pressure. The holes are then counterbored to a diameter of 1.6 mm in order to insert tubes.

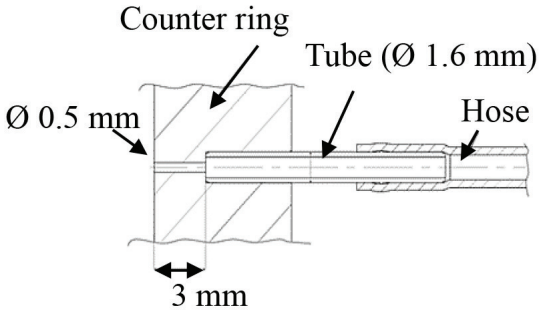

Figure 3 *Pressure hose attachment to the counter rings to measure the profile of static pressure in the gap*

The pressure holes are distributed across the surface of the counter rings in a special way. The positions of these holes are depicted in figure 4 as red dots.

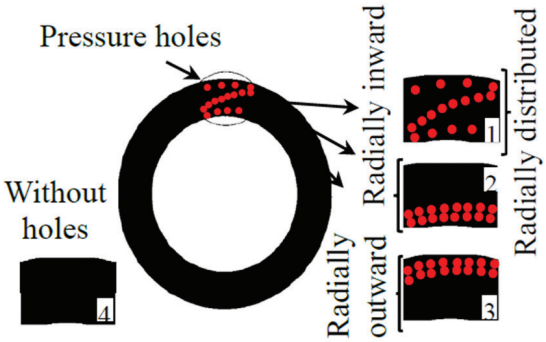

Figure 4 *Counter rings for measuring the static pressure profile in the gap*

Counter ring one has evenly distributed holes in the radial direction to allow the recording of the entire pressure profile over the ring. The other two counter rings are supposed to measure the exact pressure profiles towards the inner and outer edges of the rings. To be able to examine the influence of the pressure holes on parameters like gap height and flow rate of the process gas, a counter ring without any pressure holes is used in comparison.

Pressure measurements are conducted with a Scanivalve pressure scanner. The scanner is equipped with 16 pressure sensors having a measuring error of 0.1% FS (FS = 50 & 100 PSI).

5. LASER-BASED POWDER BED FUSION OF METALS

The laser-based powder bed fusion of metals (PBF-LB/M) process is one of many different techniques in the field of AM. This method differs in comparison with conventional methods by emergence of the component: The process takes place inside an oxygen-evacuated construction chamber. In the first manufacturing step, the powder based material is applied on a substrate plate with a height of one layer (20 µm to a maximum of 150 µm (Khorasani (2020)). Afterwards, the applied material is melted locally based on the provided CAD-model data by a laser. Thus, the part is welded on the substrate plate which is exchanged in each process. As soon as the so-called exposure process is finished, the substrate plate is lowered by the height of one layer. A coater applies material from the material stock for the next layer. Surplus material is slid into an overflow. Thus, the part arises layer by layer without the need of any part specific tool. (Bhavar et. Al. (2020), Singh et. al. (2020))

For the manufacturing process of each material, specific process parameters, like laser power, scan velocity or hatch distance are used to ensure that the material is welded without the occurrence of defects. For example, the parameter hatch distance is dependent on the width of the welding sheet, see figure 5.

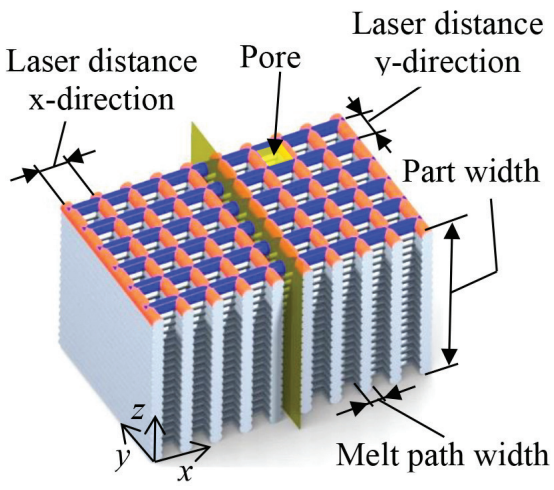

Figure 5 *Schematic illustration of the emergence of pores in the PBF-LB/M in dependence of the scan vectors and the width of the welding sheet*

Thereby, it is needed that the distance between the so-called vectors which define the path of the laser, are determined so that they overlap, and no voids are created. For the production of the permeable material, this parameter is suitable to be varied to generate defined voids which serve as pores.

6. PROTOTYPES

To validate the numerical calculation of the gap height, leakage and pressure profile in the gap for seals with varied permeabilities, prototypes with a controlled permeability over the ring surface are manufactured with the PBF-LB/M process (Variant 1). Besides the validation of the numerical calculation and the included testing of this variant, the performance is compared with one further variant (Variant 2) of seals which are already tested in a previous work:

•Variant 1: a homogeneous permeability, varied in three regions

•Variant 2: a constant homogeneous permeability distribution

Since the focus in this paper is on the distribution of the permeability, variant 2 is not discussed in detail.

The prototypes of variant 1 and variant 2 are manufactured with the laser-based powder bed fusion of metals (PBF-LB/M) process on an EOS M290 system and the material EOS GP1 which is equal to 17-4 PH (EOS (2021)).

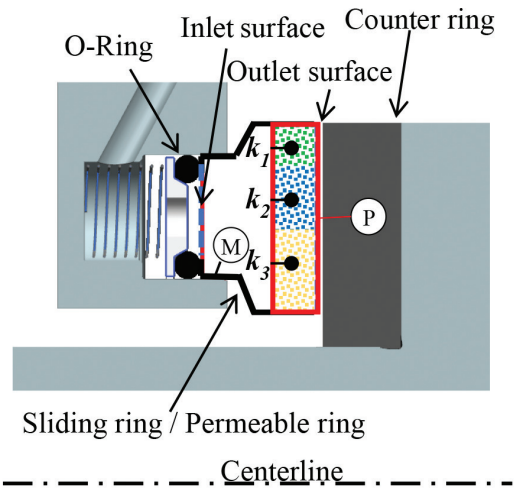

Figure 6 *Additively manufactured sliding ring with controlled average permeability*

As depicted in figure 6, the CAD- model of the PBF-LB/M manufactured rings consist of two pieces: the dense material (M) which serves as a carrier for the porous disc (P). Within the first variant of the prototypes, the porous disc is further subdivided into three parts which all have the same surface size. With this, it is possible that each of the four parts (dense, k_1, k_2, k_3) of variant 1 can be manufactured with a defined exposure strategy and thus dense or permeable material.

A solid connection between each part of the CAD-model (dense material as well as permeable material) is required to ensure the function. Therefore, there is a need for an overlap of the scan vectors. To avoid closing pores, the overlap between the porous itself and the dense material should be designed as small as possible while ensuring high strengths. Figure 7 depicts the three parts of the porous material, the scan vectors (dark blue) and the described overlap (marked area).

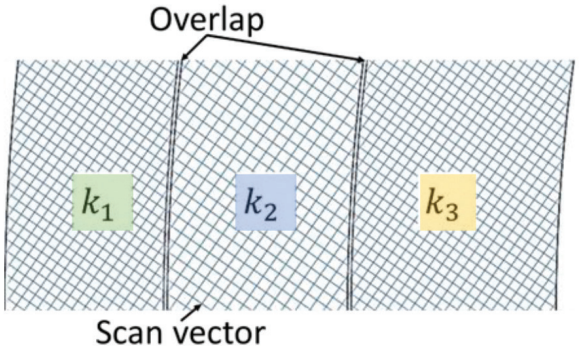

Figure 7 *Three regions of permeable material, overlap and scan vectors*

To produce the permeable material, all parameters are constant except the distance between the scan vectors of the permeable material which defines the cross-sectional area of the pores and thus the permeability, see figure 5. The PBF-LB/M parameters used for all specimens are shown in table 1.

After processing, the rings were separated from the substrate platform and functional surfaces were rotationally reworked. As performed in preliminary works, the porous surfaces were grinded, polished and lapped with low pressure to ensure that pores are not closed. Figure 8 shows the five different types of additively manufactured sliding rings with defined distribution of the permeability.

Table 1. *PBF-LB/M Process parameters for the fabrication of dense (M) and porous (P) material*

		Material	
	Unit	**M**	**P**
Scan velocity	mm/s	960	650
Laser Power	W	285	95
Hatch Distance	mm	0.09	var
Layer Height	mm	0.04	0.02

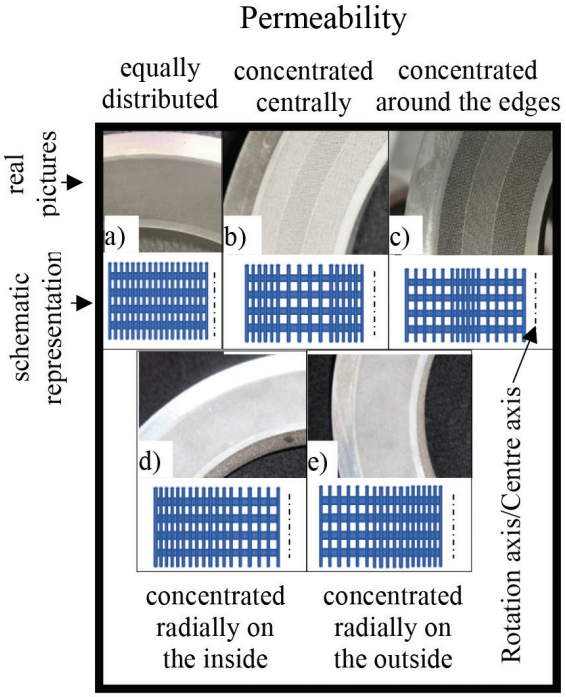

Figure 8 *Additively manufactured rings with controlled average permeability*

Type (a) has a permeability that is equally distributed across its complete surface. The permeability of the other types varies across the three zones. Each of the permeability zones of the sliding rings covers one third of the surface, meaning that the total surface area is the same as the sliding ring type with equal distribution. Thus, the direct influence of the permeability zones on the seal is investigated.

Considering the sliding rings with varying permeability zones, one type has a higher permeability concentration in the centre (b), while on another, a higher concentration of permeability is found towards the edges of the sliding ring (c). In addition, two other variations are made.

Type (d) has the highest throughput on the radial inner side and the lowest on the radial outer side, whereas for type (e), the maximum and minimum are reversed radially while the permeabilities themselves remain the same.

Table 2 shows the permeability of the sliding rings, the distribution of the permeable zones, and the corresponding ring numbers that are produced according to the numerical specification.

Table 2. *Permeability coefficients of the sliding rings examined*

Sliding ring	Variant	Type	Permeability		
			Radial inside k_3	Middle k_2	Radial outside k_1
		[-]	x 10^{-12} [m^2]		
Ring 1	2	a	950		
Ring 2	2	a	1		
Ring 3	2	a	0.9		
Ring 4	2	a	0.85		
Ring 5	2	a	0.82		
Ring 6	1	b	13,500	950	13,500
Ring 7	1	c	950	13,500	950
Ring 8	1	d	1	0.9	0.85
Ring 9	1	e	0.85	0.9	1

The permeabilities of the materials are analysed within a test series with small samples. Thereby, the volume flow, the pressure before the permeable material and the gas temperature is measured. For the calculation of the permeability, Darcy's law is used. In addition to the five different types of additively manufactured rings with constant defined permeability (Variant 2), four sliding rings (Variant 1) with distributed defined permeability, are also shown.

7. RESULTS AND VALIDATION

As shown in Schoar et al. (2021) the sliding rings create a gap that is sufficiently parallel to be able to carry out further representations by averaging the sensors signals.

Furthermore, it is also shown that only the movement of the sliding and counter rings are measured and recorded and that the environment has no influence on the measurement. To ensure that the different counter rings have no influence on the sealing properties, all were tested with sliding ring 3 between 0 bar and 5 bar differences to atmospheric pressure of the process gas. The results of these tests are shown in Figure 9.

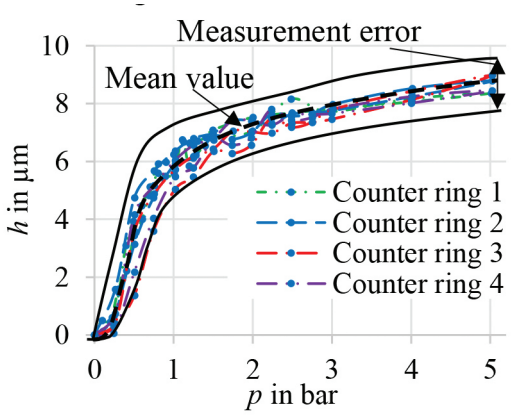

Figure 9 *Gap height development with different counter rings.*

Regardless which of the counter rings is used in the test bench, the same gap height curves are measured within the measurement tolerance. Therefore, it can be concluded that the different counter rings and the position of the pressure holes do not influence the sealing properties.

Figure 10 shows a comparison between measured and calculated characteristics of the respective seal types of the variant 1 and 2.

In the figure, the gap height is depicted versus the gas pressure in front of the rings on the inlet surface. Sliding rings 6 and 7, which are manufactured according to variant 1, have an increased gap height and thus a correspondingly higher flow rate compared to the other rings. Due to their increased permeability, seal rings 6 and 7 are not suitable for application in a turbomachine. Consequently, these sliding rings are not relevant for further consideration. A hysteresis can be seen in Figure 10 b) that can be explained by the deployed secondary seal. This secondary seal consists of two O-rings, which seal the inlet area of the primary sliding ring from the environment. To generate an initial movement of the sliding ring, the static friction of the O-rings first must be overcome.

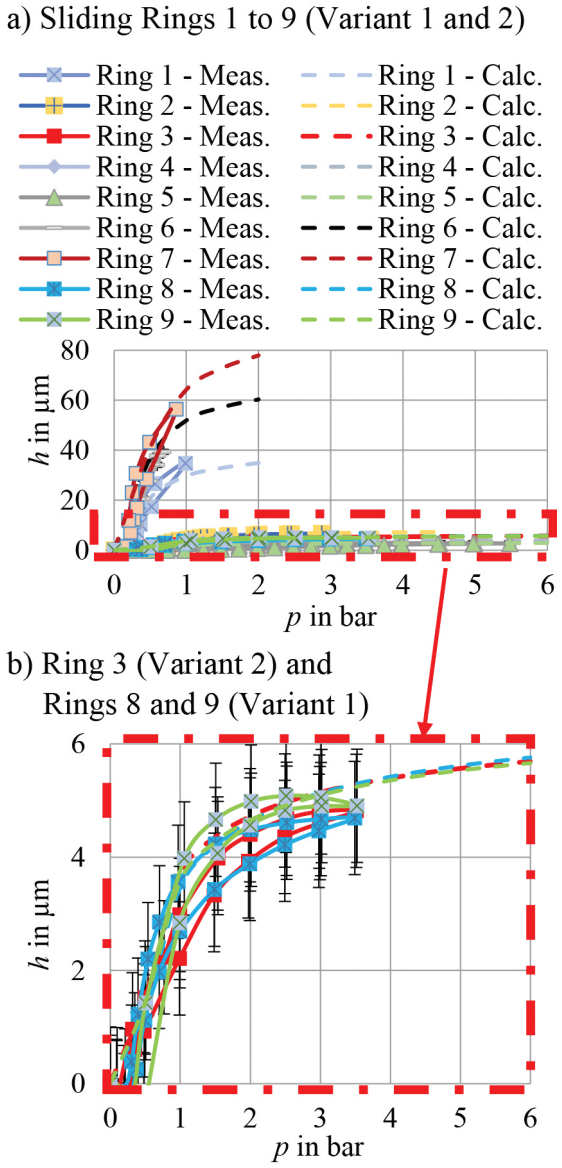

Figure 10 *Characteristics of the seals of variant 1 and 2 (measured and calculated gap height): a) all rings; b) ring 3, ring 8 and ring 9*

When the ring returns towards its initial position, the frictional forces of the O-rings are compensated by the energy stored in the springs, which creates a different balance of forces and results in the hysteresis. Furthermore, it can be seen that the gap will grow to a maximum value, depending on the permeability of the sliding ring. For reasons of simplification, the hysteresis is not taken into account in the calculation, and this accounts for the variance between the measured and calculated results. For the sliding rings with a lower gas flow (lower permeability), the calculation is more accurate than for the rings with higher trough flow (higher permeability).

This results from the higher leakage flow and the associated increase of losses of the gap flow. Due to the assumptions, the gap flow is calculated without consideration of losses. Thus, the real seal needs a smaller gap to create the same opening force as the calculated ring in the gap. When looking at Figure 10 b), it could be assumed that ring 9 drops at 2.5 bar. This is due to measurement errors when measuring the gap height.

All measured and calculated leakages of the seals manufactured according to variant 1 are depicted in figure 11. The volume flow Q (related by the maximum flow rate) is represented for the applied pressure. The graphs show that the calculation of high leakages differs. This is caused by the flow effects (such as turbulence, wall friction and pressure losses), which are not considered in the simplified calculation. As already mentioned, the focus of this work is on the smallest possible gap height, which means that the calculation is designed to be optimised for the design of a seal with low leakage.

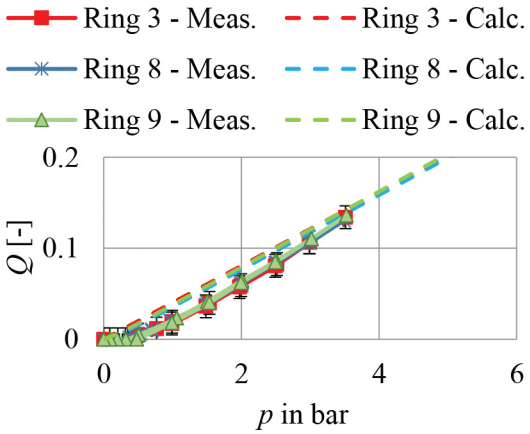

Figure 11 *Measured and calculated leakages Q of the seals manufactured according to variant 1 (rings 8 and 9) as well as to variant 2 (ring 3)*

Sliding rings 8 and 9 show the same leakage and the same maximum gap height. This can be explained by the same average permeability 9 x 10^{-13} m^2 and thus they exhibit the same opening force. Since the average permeability of these rings is very similar to ring 3 (constant permeability), it also has the same operating behaviour as thetwo rings with different permeabilities.

Diagrams a to c in figure 12 show the measured pressure profiles in the gap in comparison to the previously calculated pressure profiles.

The differences between the calculated and measured values are verry small and mostly within themeasurement error of the Scanivalve system. Another role play the manufacturing tolerances of the rings. The comparison of the results can be taken as a good validation of the numerical model.

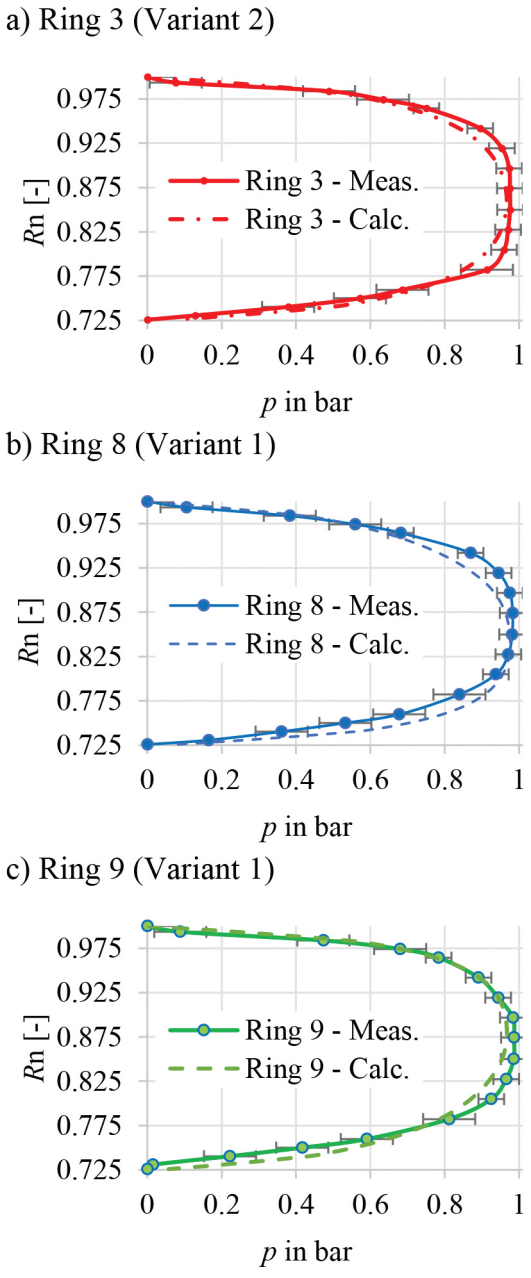

Figure 12 *Measured and calculated pressure profiles in the gap with an operating pressure of 1.0 bar for sliding rings 3, 8 and 9 in equilibrium position*

In figure 13 three measured and in figure 14 three calculated pressure profiles are plotted one above the other. The sliding rings show significant differences in their pressure profiles because of their different permeability distributions.

Considering the same operation pressure and the same geometric dimensions of the rings, the resulting pressure forces have the same value, but the local position of the point of attack is different depending on the permeability profile. This is shown by the point of attack in the calculated curves and indicated in figure 14 by vertical lines.

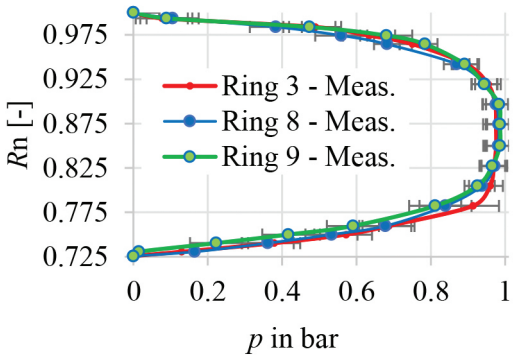

Figure 13 *Measured pressure profiles in the gap with an operating pressure of 1.0 bar for sliding rings 3, 8 and 9 in equilibrium position*

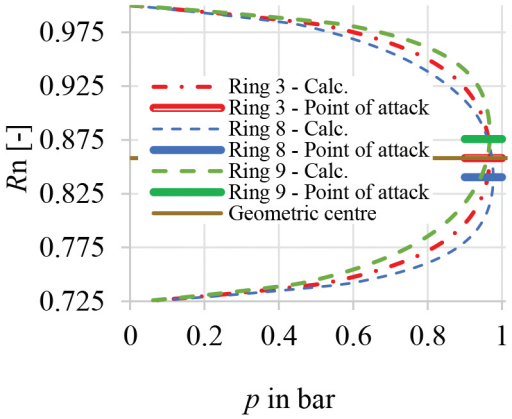

Figure 14 *Calculated pressure profiles in the gap with an operating pressure of 1.0 bar for sliding rings 3, 8 and 9 in equilibrium position*

8. CONCLUSIONS

Additive manufacturing of functional ADGS with defined distributed permeabilities and properties such as leakage or the resulting gap height can be successfully carried out in the PBF-LB/M process. The chosen strategy of fusing the parts of the CAD model in manufacturing is performing very well, so that the seals could be tested up to a pressure of 4 bar on a test bench. In this test bench, properties as the resulting gap height, the leakage of the porous sliding rings or the pressure distribution in the gap are measured.

By means of numerical calculation, the hysteresis-free properties of each aerostatic gas seal can be calculated beforehand. To validate the numerical calculation, the results are compared with the measurements from the test bench. The sliding rings manufactured according to the numerically specified permeabilities are examined. It becomes clear that the numerical calculation for the design of ADGS with defined distribution of permeabilities can be used as a tool to define the PBF-LB/M production of sliding rings. Thus, it is possible to predict typical properties of ADGS such as the gap height and the leakage as a function of the permeability and the process gas pressure.

Furthermore, not only the gap height can be predicted, but also the pressure distribution in the gap, as well as the force generated by the pressure and its point of attack.

Within the numerical calculations as well as in the experiments it can be observed that the distribution of the permeable material has a strong impact on the properties of a seal. Especially the formation of the pressure profile in the gap and thus the flow rate each direction of the process gas flow can be defined by changing the distribution respectively the value of the permeability of the seal. The PBF-LB/M technic can be used to produce complex parts and thus can optimise the functionality of ADGS.

9. OUTLOOK

Since this work opens up new areas, both theoretically and experimentally, the procedure described here gives rise to interesting ideas. The first thing standing out is the choice of materials for the sliding rings and the counter rings. A more detailed examination of additional possibilities that exist in this area or will arise in the future could contribute to a further reduction in the weight of the rings. Another aspect to be optimised against this background could also be the emergency running properties of the seal sliding rings and counter rings.

Although not explicitly investigated in this work, the possible use of this type of seal as a bearing can be considered for individual areas. In such a case, the damping and vibration behaviour would be of central importance and would have to be investigated more intensively in the future. In this context, the investigation of a fluid- structure coupling in connection with a dynamic simulation of balancing processes in combination with the autonomously occurring force equilibrium or its exact influence seems particularly promising.

10. REFERENCES

[1.] Bear, J. (1972). Dynamics of fluids in Porous Media. Dover Publications, New York.

[2.] Bhavar, V., Kattire, P., Patil, V., Khot, S., Gujar, K., & Singh, R. (2017). A review on powder bed fusion technology of metal additive manufacturing. In Additive manufacturing handbook (pp. 251-253). CRC Press.

[3.] Dagan, G. (1989). Flow and transport in porous formations. Berlin: Springer.

[4.] Darcy, H. (1856). Les fontaines publiques de la ville Dijon. Victor Dalmont.

[5.] Dormann, J. (2002). Diss. Strömungs-simulation von Luftlagern mit diskreter Düsenverteilung. Lehrstuhl für Feingeräte-bau und Getriebelehre, TU München.

[6.] EOS Website 2021, https://www.eos.info

[7.] Frene, J. N. (2005). Lubrification Hydrodynamique. Elsevier Science B.V.

[8.] Gerke M. (1991). Diss., Auslegung von ebenen und zylindrischen aerostatischen Lagern bei stationärem Betrieb. TU München.

[9.] Huber, J. (2004). Diss., Optische Druckmessung zur Untersuchung von aerostatischen Lagern. TU München.

[10.] Khorasani, A., Gibson, I., Veetil, J. K., & Ghasemi, A. H. (2020). A review of technological improvements in laser-based powder bed fusion of metal printers. International Journal of Advanced Manufacturing Technology, 108.

[11.] Launert A. (1994). Diss., Betriebssicherheit aerodynamischer Axiallager und Gleitring-dichtungen bei hohen pv-Werten. TU Carolo-Wilhelmina zu Braunschweig.

[12.] Schoar, S., Dohmen, H., & Benra, F.-K. (2019). Reliable seals for turbomachines: Numerical analysis of the effects of compressible fluid flow through porous materials and narrow gaps. In 13th European Conference on Turbomachinery Fluid Dynamics & Thermodynamics. European Turbomachinery Society.

[13.] Schoar S. Elspaß A., Kleszczynski S., Dohmen, H., & Benra, F.-K (2021). Validation of a numerical model to support the design of additively manufactured aerostatic dry gas seals carried out on a test bench through use of seals with defined permeabilities. In 14th European Conference on Turbomachinery Fluid Dynamics & Thermodynamics. European Turbomachinery Society.

[14.] Schroter, A. (1994). Diss., Ausgleichs-vorgänge und Strömungsgeräusche bei aerostatischen Lagern mit flächig verteilten Mikrodüsen. TU München.

[15.] Schulz B. (1999). Diss., Herstellung von aerostatischen Lagern mit Laserend-bearbeitung. TU München. VDI-Verlag - Düsseldorf.

[16.] Singh, R., Gupta, A., Tripathi, O., Srivastava, S., Singh, B., Awasthi, A., Rajput, S.K., Sonia, P., Singhal, P., Saxena, K. K. (2020). Powder bed fusion process in additive manufacturing: An overview. Materials Today: Proceedings 26, 3058-3070.

Correspondence
Schaham.Schoar@uni-due.de